# Radio/X-Ray Correlation in the Mini-outbursts of Black Hole X-Ray Transient GRS 1739–278

Fu-Guo Xie[1] , Zhen Yan[1] , and Zhongzu Wu[2]

[1] Key Laboratory for Research in Galaxies and Cosmology, Shanghai Astronomical Observatory, Chinese Academy of Sciences, 80 Nandan Road, Shanghai 200030, People's Republic of China; fgxie@shao.ac.cn, zyan@shao.ac.cn
[2] College of Science, Guizhou University, Guiyang 550025, Guiyang, People's Republic of China; zzwu08@gmail.com
*Received 2019 November 7; revised 2020 January 26; accepted 2020 January 27; published 2020 March 2*

## Abstract

We present quasi-simultaneous radio and X-ray observations of the black hole X-ray binary GRS 1739–278 during the 2015–2016 mini-outbursts, i.e., between 2015 June 10 and 2016 October 31, with the X-ray-to-radio time interval being less than one day. The monitor campaign was run by *Swift* in the X-rays and by VLA in the radio (at both 5 and 8 GHz). We find that the brightest radio emission is actually achieved during the soft sate, and the spectrum is marginally optically thick with the spectral index $\alpha \approx -0.28 \pm 0.17$ (flux $F_\nu \propto \nu^\alpha$). For the radio emission in the hard state, we find a large diversity in the spectral index, i.e., a majority of radio spectra are optically thick with $-0.5 \lesssim \alpha \lesssim 0.5$, while a few are optically thin, with $\alpha$ being lower than $-1$ in certain cases. We then investigate the correlation between the luminosities in radio (monochromatic at 5 GHz, $L_R$) and 1–10 keV X-rays ($L_X$) during the hard state. We find that for more than two orders of magnitude variation in the X-ray luminosity, this source exhibits a flat correlation with $p \approx 0.16$ (in the form of $L_R \propto L_X^p$), i.e., it belongs to the "outlier" (to the standard correlation with $p \approx 0.6$) category that may follow a hybrid correlation. Both the slope and the corresponding luminosity range agree well with those in H1743–322, the prototype of the hybrid correlation. Theoretical implications of our results are discussed.

*Unified Astronomy Thesaurus concepts:* Stellar accretion disks (1579); Black hole physics (159); X-ray binary stars (1811); Low-mass x-ray binary stars (939)

## 1. Introduction

A majority of stellar-mass black hole (BH) X-ray binaries (BHBs) are transients. After a long period of quiescence, they occasionally undergo outbursts. According to the spectral and timing properties, two distinctive states are identified (Zdziarski & Gierliński 2004; Remillard & McClintock 2006; Done et al. 2007; Belloni 2010). One is the soft state, in which the X-ray spectrum is dominated by thermal component from the cold accretion disk (Shakura & Sunyaev 1973), and is supplemented by a weak power-law tail with photon index $\Gamma > 2.1$ (X-ray spectrum defined as $F_\nu \propto \nu^{1-\Gamma}$) hard X-rays. The other is the hard state, in which the X-ray spectrum is dominated by emission from the Compton scattering within hot accretion flows, while the thermal emission becomes much weaker. Observationally, the Comptonized emission is shown as a $\Gamma \approx 1.4$–1.8 power-law emission which has an exponential high-energy cutoff at around ~100 keV (e.g., Zdziarski et al. 1998). Additionally when the thermal and the nonthermal emissions are of comparable significance, it is defined as the intermediate state, which is further divided into hard inter-mediate and soft intermediate states.

BHBs in their hard state are ubiquitous with compact self-absorbed radio emission that originates from a highly collimated relativistic jet (for reviews, see Corbel et al. 2004; Fender et al. 2004, 2009; Fender & Gallo 2014). This so-called "continuous jet" or "steady jet" has an optically thick radio spectrum, with $\alpha \sim 0$ (defined as flux $F_\nu \propto \nu^\alpha$; flat or slightly inverted, i.e., $-0.5 \lesssim \alpha \lesssim 0.5$). During the hard-to-soft state transition, the continuous jet switches off (being quenched by a factor of $\gtrsim 100$ in the radio band; e.g., Fender et al. 1999; Coriat et al. 2011; Russell et al. 2011, 2019). Meanwhile, discrete bright knots/plasmoids are observed to move outward

relativistically (e.g., Mirabel & Rodriguez 1994; Hjellming & Rupen 1995; Fender et al. 1999; Yang et al. 2010; Russell et al. 2019). These plasmoids are interpreted as the "episodic jet" or "transient jet," and their radio emission is optically thin ($\alpha < -0.5$; steep spectrum)[3] and highly polarized (see, e.g., Fender et al. 2004, 2009; Yuan et al. 2009a; Zhang & Yu 2015 for summaries). In the soft state, the continuous jet is always quenched, while residuals of the episodic ejecta (created during the hard-to-soft state transition) may still exist (e.g., Brocksopp et al. 2013), possibly due to the interactions between the ejecta and the surrounding environment (e.g., Corbel et al. 2002).

A fundamental tool in investigating the disk–jet connection is to probe the correlation between radio (monochromatic, $L_R = \nu L_\nu$ at, e.g., 5 GHz) and X-ray (integrated, i.e., $L_X = \int L_\nu d\nu$ in e.g., the 1–10 keV band) luminosities based on their quasi-simultaneous measurements in the hard state (Corbel et al. 2000, 2003, 2013; Gallo et al. 2003, 2012, 2014; Fürst et al. 2015; Plotkin et al. 2017; Islam & Zdziarski 2018; Rodriguez et al. 2020). It is found that the radio and X-ray luminosities follow a tight nonlinear correlation (hereafter RX correlation), $L_R \propto L_X^p$ with the slope index $p \approx 0.6 \pm 0.1$ (Corbel et al. 2003, 2013).[4] This represents the standard RX correlation (see the black dashed curve in Figure 4). With the BH mass $M_{BH}$ introduced as a new factor, this correlation was later extended to include low-luminosity active galactic nuclei (AGNs) also, and it is renamed the fundamental plane of BH activity in logarithmic space (e.g., Merloni et al. 2003; Falcke

---

[3] For the spectral property of the radio emission, we use optically thin/steep/ $\alpha < -0.5$ interchangably, and optically thick/flat/$-0.5 \lesssim \alpha \lesssim 0.5$ inter-changably as well.
[4] A slight offset in the normalization among the full and failed (defined as the case of no transition into the soft state) outbursts are observed in GX 339-4 (Fürst et al. 2015).

et al. 2004; Wang et al. 2006; Panessa et al. 2007; Li et al. 2008; Gültekin et al. 2009, 2019; Qian et al. 2018; Li & Gu 2018). With an emphasis on the slope $p$ instead of the dependence on $M_{BH}$, below for simplicity it will still be referred to as the RX correlation.

Since the discovery, the empirical standard RX correlation is broadly established among a majority of sources. However, different correlation slope $p$ is reported in some specified systems, e.g., the radio-loud AGNs (Wang et al. 2006; Panessa et al. 2007; Li et al. 2008), the narrow-line Seyfert 1 galaxies (Yao et al. 2018), and the faint/quiescent AGNs (Yuan et al. 2009b; Xie & Yuan 2017, but see Mezcua et al. 2018).[5] Even within its typical dynamical range, sources with clear deviations to the standard RX correlation are observed in both BHBs (so-called "outliers" for BHBs, e.g., Corbel et al. 2004; Coriat et al. 2011; Jonker et al. 2012; Brocksopp et al. 2013; Dong et al. 2014) and AGNs (e.g., Bell et al. 2011; King et al. 2011, 2013; Xie et al. 2016). As demonstrated in the prototype BHB H1743–322 (Coriat et al. 2011) and low-luminosity AGN NGC 7213 (Bell et al. 2011; Xie et al. 2016), these outliers likely follow a hybrid correlation, i.e., a steep $p \approx 1.3$–1.4 branch at the bright $L_X$ regime (see the blue dotted–dashed curve in Figure 4) and $p \sim 0$ branch at the moderate $L_X$ regime. Hint on the recovery back to the standard correlation is also observed in H1743–322 when it is sufficiently weak in $L_X$ (Coriat et al. 2011). We note that the existence of a new RX correlation track is also confirmed from statistics, i.e., through the data-cluster analysis method Gallo et al. (2012) find from a sample of 18 BHBs that, besides the standard one, there exists another $p \approx 0.98$ correlation at the $L_X > 10^{36}$ erg s$^{-1}$ regime.

Physically, the standard RX correlation provides strong evidence for a tight connection between the hot X-ray emitting source (usually a hot accretion flow), and the radio source (usually a continuous jet), and it is understood under the coupled accretion–jet model, where a scale-invariant jet model is considered (e.g., Heinz & Sunyaev 2003; Merloni et al. 2003; Heinz 2004; Yuan & Cui 2005; Xie & Yuan 2016). The physics behind the hybrid RX correlation, as well as its connection to the standard one, on the other hand, remain unclear. One promising solution is to attribute the change in the correlation slope $p$ to the change in the mode of hot accretion flows (rather than that in jet physics; see Xie & Yuan 2016 and Section 4.3). Alternative models for the $p \approx 1.3$–1.4 branch can be found in Meyer-Hofmeister & Meyer (2014), Cao et al. (2014), Qiao & Liu (2015), and alternative models for the $p \sim 0$ branch can be found in Islam & Zdziarski (2018) and Espinasse & Fender (2018). For completeness, we note that the episodic jet, which is typically associated with the state transition, may have a different origin. Likely it relates to the formation and catastrophic disruption of the magnetic flux rope above the surface of accretion flow, see Yuan et al. (2009a) for details.

In this work we focus on the the 2015–2016 mini-outbursts of the X-ray transient GRS 1739–278. Located at a distance of 6–8.5 kpc (Greiner et al. 1996; Yan & Yu 2017b), the binary system has an inclination of $i \approx 32°.5$ (Miller et al. 2015). It was discovered in 1996 by the SIGMA gamma-ray telescope on board the *Granat* satellite (Vargas et al. 1997), and is

classified as a BH candidate based on the similarities in spectral and timing properties to other BHBs, as well as the detection of a strong quasi-periodic oscillation in the intermediate state (Borozdin & Trudolyubov 2000). Eighteen years later, in 2014 GRS 1739–278 underwent a new main outburst (Krimm et al. 2014), whose duration is remarkably long, i.e., more than one year. The peak X-ray luminosity of the 2014 outburst reaches $\sim 5 \times 10^{38}$ erg s$^{-1}$ (Yan & Yu 2017b; Wang et al. 2018). Thanks to the intense X-ray monitoring of *Swift* afterwards, a series of mini-outbursts have been discovered, where state transitions are also detected in the first two mini-outbursts (see Yan & Yu 2017a, 2017b and also Figure 1).

This work is organized as follows. In Section 2 we report the data analysis of these mini-outbursts, while in Section 3 we compile these data and investigate the radio properties. We find this source follows a flat RX correlation, for more than two orders of magnitude in the variation of X-ray luminosity. A discussion with a brief summary is given in Section 4. Throughout this work, the distance of GRS 1739–278 is fixed to $d = 7.5$ kpc (Yan & Yu 2017b).

## 2. Observation and Data Reduction

After a main outburst in 2014, GRS 1739–278 underwent a series of mini-outbursts. These mini-outbursts are fainter by a factor of $\gtrsim$10–30 to the main outburst in 2014, and have been monitored with a moderate cadence by *Swift* (Yan & Yu 2017a, 2017b; Parikh et al. 2018). As listed in detail in Table 1, it is also covered by the Karl G. Jansky Very Large Array (VLA) at 32 epochs (see Section 3.1 later). Since we are mostly interested in the RX correlation, we only consider quasi-simultaneous observations, where the X-ray-to-radio time interval is required to be less than one day. With this quasi-simultaneity requirement, we only have 25 pairs of observations.

Table 1 shows the details of all the observations. In the radio part we include the observation date (the modified Julian date, MJD) and fluxes at two wavebands. The spectral index in radio is also provided. In the X-ray part we include the observation ID and the date of *Swift*/XRT observations, the exposure time, the X-ray flux and the spectral state of the system. The exact time interval between radio and X-ray observations can then be derived easily.

### 2.1. Swift/XRT Observation and Spectral Analysis

The data reduction and analysis in X-rays are done through standard procedures, i.e., the *Swift*/XRT event data were first processed with XRTPIPELINE (v 0.13.2) to generate the cleaned event data, and then grade 0 events are extracted by XSELECT. For those with high count rate (>0.6 counts s$^{-1}$ for the photon counting mode, and >150 counts s$^{-1}$ for the windowed timing mode), the events in the central region that suffer pile-up effect are excluded. The details can be found in Yan & Yu (2017b). Below we provide a brief description on the spectral modeling.

The X-ray spectrum is modeled by an absorbed power-law component from the hot accretion flow, and a thermal component from the cold disk, i.e., *tbabs∗(powerlaw+diskbb)* in XSPEC notation. The hydrogen column density $N_H$ of the absorption in soft X-rays is constrained to be $\approx 2.5 \times 10^{22}$ cm$^{-2}$, which is in good agreement with individual measurements by *XMM–Newton* and *NuSTAR* (Miller et al.

---

[5] Quiescent BHBs seem to follow the standard RX correlation (Gallo et al. 2014; Plotkin et al. 2017), maybe because they are still not dim enough in these observations (e.g., see discussions in Xie & Yuan 2017, and a hint in Dincer et al. 2018; Rodriguez et al. 2020).
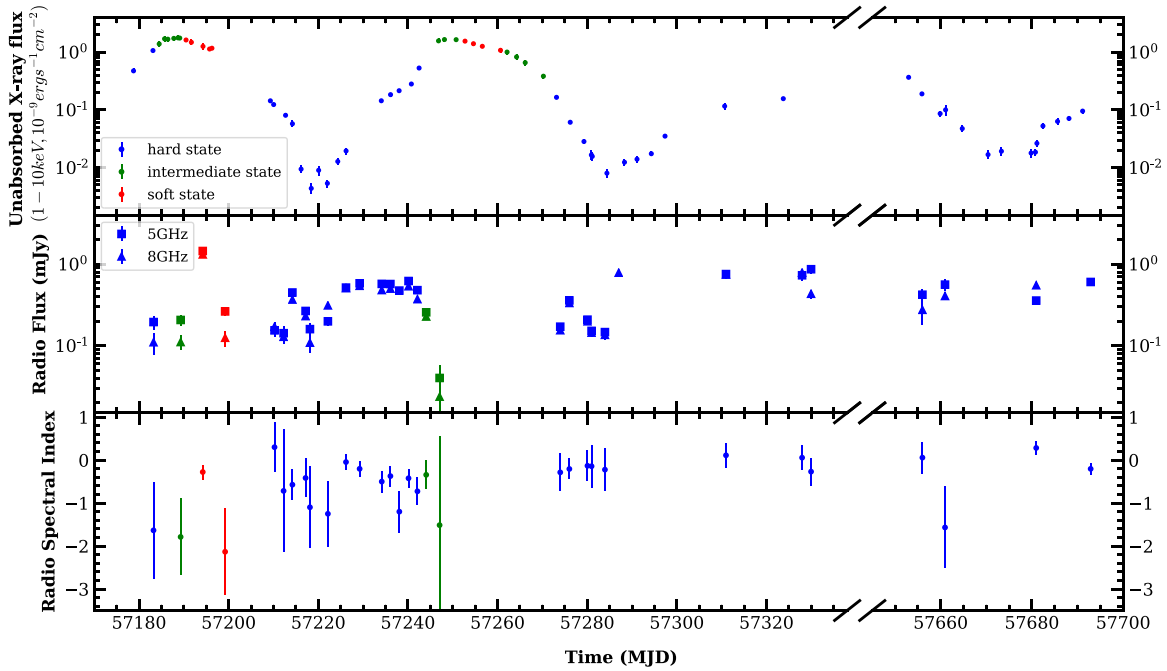
**Figure 1.** Light curves in X-rays (1–10 keV, top panel) and radio (middle panel). The bottom panel shows the spectral index $\alpha$ in radio. In all the panels, the accretion states are shown in color, i.e., the soft state in red, the hard state in blue, and the intermediate state in green. In the middle panel, the filled squares are at either 5.26 GHz (i.e., before MJD 57330) or 4.70 GHz (i.e., after MJD 57656), while the filed triangles are at 7.45 GHz. See Section 2.2 for details.

2015; Fürst et al. 2016). The spectral state is of crucial importance for our investigation. We follow Remillard & McClintock (2006) and Belloni (2010) to define the hard state if the emission is dominated by a power-law component whose X-ray photon index is also less than 2.1, the soft state as the flux contribution from disk thermal component being larger than 80%, and the in-between spectra are defined as in the intermediate state (see also Yan & Yu 2017a). Note that thanks to the intense monitoring in X-rays, 25 epochs out of the total 32 radio observations have quasi-simultaneous X-ray observations, thus their accretion states can be clearly determined. For the rest of the (7/32) radio epochs that lack the X-ray information, their accretion state is constrained/estimated based on the evolutionary trend as well as X-ray observations at two adjacent epochs (epochs before and after the radio observation). Take MJD 57229 as an example. X-ray monitoring indicates that GRS 1739–278 is in the hard state during the period of MJD 57220–57243 (more specifically, on MJD 57226 and MJD 57234, see Figure 1 and Yan & Yu 2017a). We thus argue that GRS 1739–278 is also in the hard state on MJD 57229, as listed in Table 1.

We calculate the 1–10 keV X-ray flux from the spectral fitting by the model *cflux*, which are shown in the top panel of Figure 1 (and Table 1), where uncertainties in the flux are evaluated at 90% confidence. At least five mini-outbursts are captured by *Swift*/XRT, among which the first two have monitoring in both the rise and the decay phases. The dynamical range in X-rays is almost three orders of magnitude, between $\sim 4 \times 10^{-12}$ and $\sim 2 \times 10^{-9}$ erg s$^{-1}$ cm$^{-2}$. Even for those hard states with radio data only, the dynamical range in X-rays is still more than two orders of magnitude.

### 2.2. VLA Radio Observation and Data Reduction

Radio observations of GRS 1739–278 were obtained by VLA (Project code VLA/SB4161 and SH0281, PI: S. Corbel)

between 2015 June 10 and 2016 October 31, with a total of 32 epochs. The time interval between two neighboring radio epochs varies, with a typical value of $\approx 2.5$–5 days during the first two mini-outbursts (see Table 1 and Figure 1). It is observed at C band, simultaneously centering at two broad frequencies (hereafter subbands). One subband centers at 7.45 GHz, and the other centers at either 5.26 GHz (2015 June 10–2015 November 3, i.e., before MJD 57330) or 4.70 GHz (2016 September 25–2016 October 31, i.e., since MJD 57656). Both subbands have a bandwidth of 1 GHz, i.e., the total bandwidth is 2 GHz. The on-source exposure time varies between 18 and 80 minutes. The VLA observations are in the A configuration, with a typical spatial resolution (full width at half maximum, FWHM) of about 900 mas × 350 mas at 5 GHz and of about 650 mas × 250 mas at 7.45 GHz (mas is the abbreviation of milliarcsecond; see Figure 2).

The calibration was performed using the standard VLA pipeline of the Common Astronomy Software Application v5.4.1 (CASA, McMullin et al. 2007). After calibration, the data of target sources is split and exported out (in fits format). Further processes including the imaging are done in Difmap software (Shepherd et al. 1994). Depending on exposure time and wavelength, the $1\sigma_{\rm rms}$ sensitivity we achieved varies between $\approx 6\ \mu$Jy beam$^{-1}$ and $\approx 50\ \mu$Jy beam$^{-1}$. Finally, the flux density at each epoch is derived by fitting a point source in the image plane using the task MODELFIT, and the results are summarized in Table 1. We note that for the 5.26 GHz observation on 2015 September 22 (MJD 57287), all of the calibrated data is flagged out after the pipeline reduction, and is thus not considered in our data analysis. For the uncertainties of the radio flux reported in Table 1, we follow Nyland et al. (2017) to include both $\sigma_{\rm rms}$ of the image and a systematic 3% uncertainty in the absolute flux density scale, i.e., we have $\sigma_{\rm tot} = \sqrt{(2\,\sigma_{\rm rms})^2 + (0.03\,S_{\rm peak})^2}$, where $S_{\rm peak}$ is the peak intensity (flux per beam).

**Table 1**
Quasi-simultaneous VLA and *Swift*/XRT Observations of GRS 1739–278

| VLA | | | | *Swift*/XRT | | | | |
| --- | --- | --- | --- | --- | --- | --- | --- | --- |
| Date (MJD) | $F_5$ (mJy) | $F_8$ (mJy) | Spectral Index $\alpha$ | ObsID | Date (MJD) | Exposure (s) | $F_X$ (erg s$^{-1}$ cm$^{-2}$) | State |
| 57183.23 | $0.19^{+0.04}_{-0.04}$ | $0.11^{+0.03}_{-0.03}$ | $-1.63^{+1.12}_{-1.12}$ | 00033812002 | 57183.11 | 869.61 | $1.07^{+0.02}_{-0.02} \times 10^{-9}$ | Hard |
| 57189.28 | $0.21^{+0.03}_{-0.03}$ | $0.11^{+0.02}_{-0.02}$ | $-1.79^{+0.89}_{-0.89}$ | 00033812008 | 57189.08 | 984.61 | $1.76^{+0.14}_{-0.14} \times 10^{-9}$ | Intermediate |
| 57194.21 | $1.45^{+0.05}_{-0.05}$ | $1.32^{+0.05}_{-0.05}$ | $-0.28^{+0.17}_{-0.17}$ | 00033812013 | 57194.27 | 619.58 | $1.26^{+0.16}_{-0.16} \times 10^{-9}$ | Soft |
| 57199.20 | $0.26^{+0.03}_{-0.03}$ | $0.12^{+0.03}_{-0.03}$ | $-2.13^{+1.00}_{-1.00}$ | ⋯ | ⋯ | ⋯ | ⋯ | Soft? |
| 57210.23 | $0.15^{+0.03}_{-0.03}$ | $0.17^{+0.02}_{-0.02}$ | $0.30^{+0.58}_{-0.58}$ | 00033812017 | 57210.03 | 1892.36 | $1.24^{+0.06}_{-0.06} \times 10^{-10}$ | Hard |
| 57212.25 | $0.14^{+0.03}_{-0.03}$ | $0.11^{+0.04}_{-0.04}$ | $-0.72^{+1.43}_{-1.43}$ | 00033812018 | 57212.69 | 1293.76 | $8.06^{+0.63}_{-0.63} \times 10^{-11}$ | Hard |
| 57214.22 | $0.45^{+0.03}_{-0.03}$ | $0.37^{+0.03}_{-0.03}$ | $-0.57^{+0.35}_{-0.35}$ | 00033812019 | 57214.22 | 1534.21 | $5.75^{+0.70}_{-0.70} \times 10^{-11}$ | Hard |
| 57217.16 | $0.27^{+0.03}_{-0.03}$ | $0.23^{+0.03}_{-0.03}$ | $-0.42^{+0.44}_{-0.44}$ | 00033812020 | 57216.16 | 1969.95 | $9.41^{+1.31}_{-1.31} \times 10^{-12}$ | Hard |
| 57218.13 | $0.16^{+0.03}_{-0.03}$ | $0.11^{+0.03}_{-0.03}$ | $-1.10^{+0.95}_{-0.95}$ | 00033812021 | 57218.42 | 2153.76 | $4.37^{+0.93}_{-0.93} \times 10^{-12}$ | Hard |
| 57222.14 | $0.20^{+0.02}_{-0.02}$ | $0.13^{+0.02}_{-0.02}$ | $-1.25^{+0.76}_{-0.76}$ | 00033812023 | 57222.02 | 2127.87 | $5.34^{+0.84}_{-0.84} \times 10^{-12}$ | Hard |
| 57226.17 | $0.52^{+0.02}_{-0.02}$ | $0.51^{+0.02}_{-0.02}$ | $-0.05^{+0.18}_{-0.18}$ | 00033812025 | 57226.20 | 935.22 | $1.95^{+0.25}_{-0.25} \times 10^{-11}$ | Hard |
| 57229.22 | $0.58^{+0.03}_{-0.03}$ | $0.54^{+0.02}_{-0.02}$ | $-0.20^{+0.18}_{-0.18}$ | ⋯ | ⋯ | ⋯ | ⋯ | Hard |
| 57234.16 | $0.57^{+0.03}_{-0.03}$ | $0.48^{+0.02}_{-0.02}$ | $-0.50^{+0.25}_{-0.25}$ | 00033812026 | 57234.06 | 3745.90 | $1.44^{+0.06}_{-0.06} \times 10^{-10}$ | Hard |
| 57236.08 | $0.57^{+0.03}_{-0.03}$ | $0.50^{+0.03}_{-0.03}$ | $-0.37^{+0.23}_{-0.23}$ | 00033812027 | 57236.12 | 3457.74 | $1.84^{+0.12}_{-0.12} \times 10^{-10}$ | Hard |
| 57238.08 | $0.47^{+0.03}_{-0.03}$ | $0.31^{+0.02}_{-0.02}$ | $-1.20^{+0.48}_{-0.48}$ | 00033812028 | 57238.03 | 3708.70 | $2.15^{+0.08}_{-0.08} \times 10^{-10}$ | Hard |
| 57240.13 | $0.62^{+0.03}_{-0.03}$ | $0.54^{+0.02}_{-0.02}$ | $-0.42^{+0.21}_{-0.21}$ | 00033812029 | 57240.76 | 3978.57 | $2.81^{+0.14}_{-0.14} \times 10^{-10}$ | Hard |
| 57242.11 | $0.48^{+0.02}_{-0.02}$ | $0.37^{+0.02}_{-0.02}$ | $-0.73^{+0.31}_{-0.31}$ | 00033812030 | 57242.49 | 4111.97 | $5.31^{+0.17}_{-0.17} \times 10^{-10}$ | Hard |
| 57244.07 | $0.26^{+0.02}_{-0.02}$ | $0.23^{+0.02}_{-0.02}$ | $-0.34^{+0.33}_{-0.33}$ | ⋯ | ⋯ | ⋯ | ⋯ | Intermediate? |
| 57247.06 | $0.04^{+0.02}_{-0.02}$ | $0.02^{+0.01}_{-0.01}$ | $-1.51^{+2.07}_{-2.07}$ | 00033812032 | 57246.82 | 1844.34 | $1.57^{+0.14}_{-0.14} \times 10^{-9}$ | Intermediate |
| 57273.98 | $0.17^{+0.02}_{-0.02}$ | $0.15^{+0.02}_{-0.02}$ | $-0.28^{+0.44}_{-0.44}$ | 00033812043 | 57273.15 | 1448.96 | $1.65^{+0.07}_{-0.07} \times 10^{-10}$ | Hard |
| 57276.02 | $0.36^{+0.02}_{-0.02}$ | $0.33^{+0.02}_{-0.02}$ | $-0.21^{+0.24}_{-0.24}$ | 00033812044 | 57276.21 | 1948.78 | $6.11^{+0.40}_{-0.40} \times 10^{-11}$ | Hard |
| 57280.06 | $0.21^{+0.02}_{-0.02}$ | $0.20^{+0.02}_{-0.02}$ | $-0.13^{+0.36}_{-0.36}$ | 00033812045 | 57279.27 | 2139.22 | $2.83^{+0.24}_{-0.24} \times 10^{-11}$ | Hard |
| 57280.97 | $0.15^{+0.02}_{-0.02}$ | $0.14^{+0.02}_{-0.02}$ | $-0.14^{+0.50}_{-0.50}$ | 00081764002 | 57280.93 | 914.03 | $1.66^{+0.31}_{-0.31} \times 10^{-11}$ | Hard |
| 57283.95 | $0.15^{+0.02}_{-0.02}$ | $0.14^{+0.02}_{-0.02}$ | $-0.22^{+0.49}_{-0.49}$ | 00033812046 | 57284.40 | 2162.19 | $8.01^{+1.30}_{-1.30} \times 10^{-12}$ | Hard |
| 57287.02 | ⋯ | $0.19^{+0.03}_{-0.03}$ | ⋯ | ⋯ | ⋯ | ⋯ | ⋯ | Hard |
| 57310.97 | $0.76^{+0.09}_{-0.09}$ | $0.79^{+0.05}_{-0.05}$ | $0.11^{+0.29}_{-0.29}$ | 00033812052 | 57310.67 | 1813.58 | $1.16^{+0.16}_{-0.16} \times 10^{-10}$ | Hard |
| 57327.95 | $0.73^{+0.10}_{-0.10}$ | $0.74^{+0.05}_{-0.05}$ | $0.06^{+0.29}_{-0.29}$ | ⋯ | ⋯ | ⋯ | ⋯ | Hard |
| 57329.95 | $0.87^{+0.10}_{-0.10}$ | $0.79^{+0.06}_{-0.06}$ | $-0.27^{+0.32}_{-0.32}$ | ⋯ | ⋯ | ⋯ | ⋯ | Hard |
| 57656.00 | $0.42^{+0.07}_{-0.07}$ | $0.43^{+0.05}_{-0.05}$ | $0.06^{+0.37}_{-0.37}$ | 00033812056 | 57655.89 | 965.91 | $1.90^{+0.12}_{-0.12} \times 10^{-10}$ | Hard |
| 57660.95 | $0.56^{+0.09}_{-0.09}$ | $0.28^{+0.10}_{-0.10}$ | $-1.57^{+0.95}_{-0.95}$ | 00033812058 | 57661.07 | 748.76 | $1.00^{+0.20}_{-0.20} \times 10^{-10}$ | Hard |
| 57680.93 | $0.36^{+0.02}_{-0.02}$ | $0.41^{+0.02}_{-0.02}$ | $0.28^{+0.16}_{-0.16}$ | 00081979002 | 57681.08 | 1903.88 | $2.64^{+0.32}_{-0.32} \times 10^{-11}$ | Hard |
| 57692.86 | $0.60^{+0.02}_{-0.02}$ | $0.55^{+0.02}_{-0.02}$ | $-0.20^{+0.13}_{-0.13}$ | ⋯ | ⋯ | ⋯ | ⋯ | Hard |

**Note.** $F_5$ represents radio flux at 5.26 GHz (2015 June 10–2015 November 3, i.e., before MJD 57330) or 4.70 GHz (2016 September 25–2016 October 31, i.e., since MJD 57656). $F_8$ and $F_X$ are the radio and X-ray fluxes, respectively, at 7.45 GHz and between 1 and 10 keV.

Once the fluxes at two frequencies are measured, we can then evaluate the spectral index $\alpha$ (see the bottom panel of Figure 1), where the uncertainty in the frequency because of the broad 1 GHz bandwidth is also taken into account.

### 3. Results

The X-ray lightcurve of GRS 1739–278 of the 2015–2016 mini-outbursts is shown in the top panel of Figure 1. The X-ray properties are analyzed and discussed in detail in Yan & Yu (2017b). As shown in the top panel of Figure 1, state transitions, typically observed in the main outbursts, are also observed in the first two mini-outbursts. Note that Yan & Yu (2017b) found that the much-fainter soft state in mini-outbursts likely follows the same tight $L_{\rm bol} \propto T^4$ (bolometric luminosity $L_{\rm bol}$ and representative temperature of the cold disk $T$) relationship as determined by that in the major 2014 outburst, suggesting that the cold disk is also not truncated in these soft states of mini-outbursts.

Below we focus on the radio observations and the disk–jet coupling.

### 3.1. Image and Spectral Properties in Radio

The spatial morphology of GRS 1739–278 remains compact (i.e., unresolved) among almost all our A-configuration VLA observations. For illustrative purposes we show in Figure 2 the image at 5.26 GHz (top panels) and 7.45 GHz (bottom panels) in three different states, i.e., in hard state on 2015 June 10 (MJD 57183, left panels), in intermediate state on 2015 June 16 (MJD 57189, middle panels), and in soft state on 2015 June 21 (MJD 57194, right panels). In all the plots, the central position locates at R.A. = $17^{\rm h}42^{\rm m}40\overset{s}{.}030$ and decl. = $-27°44'52\overset{''}{.}699$ in the J2000 coordinate, which is determined by the VLA observation (in C configuration) of its 1996 outburst (Durouchoux et al. 1996). We do not observe any offset in the position (in either R.A. or decl.) in any spectral states, even in the intermediate and soft states where episodic ejections with superluminal motions are commonly observed (for superluminal ejections, see, e.g., Mirabel & Rodriguez 1994; Hjellming & Rupen 1995; Fender et al. 1999; Yang et al. 2010; Russell et al. 2019).
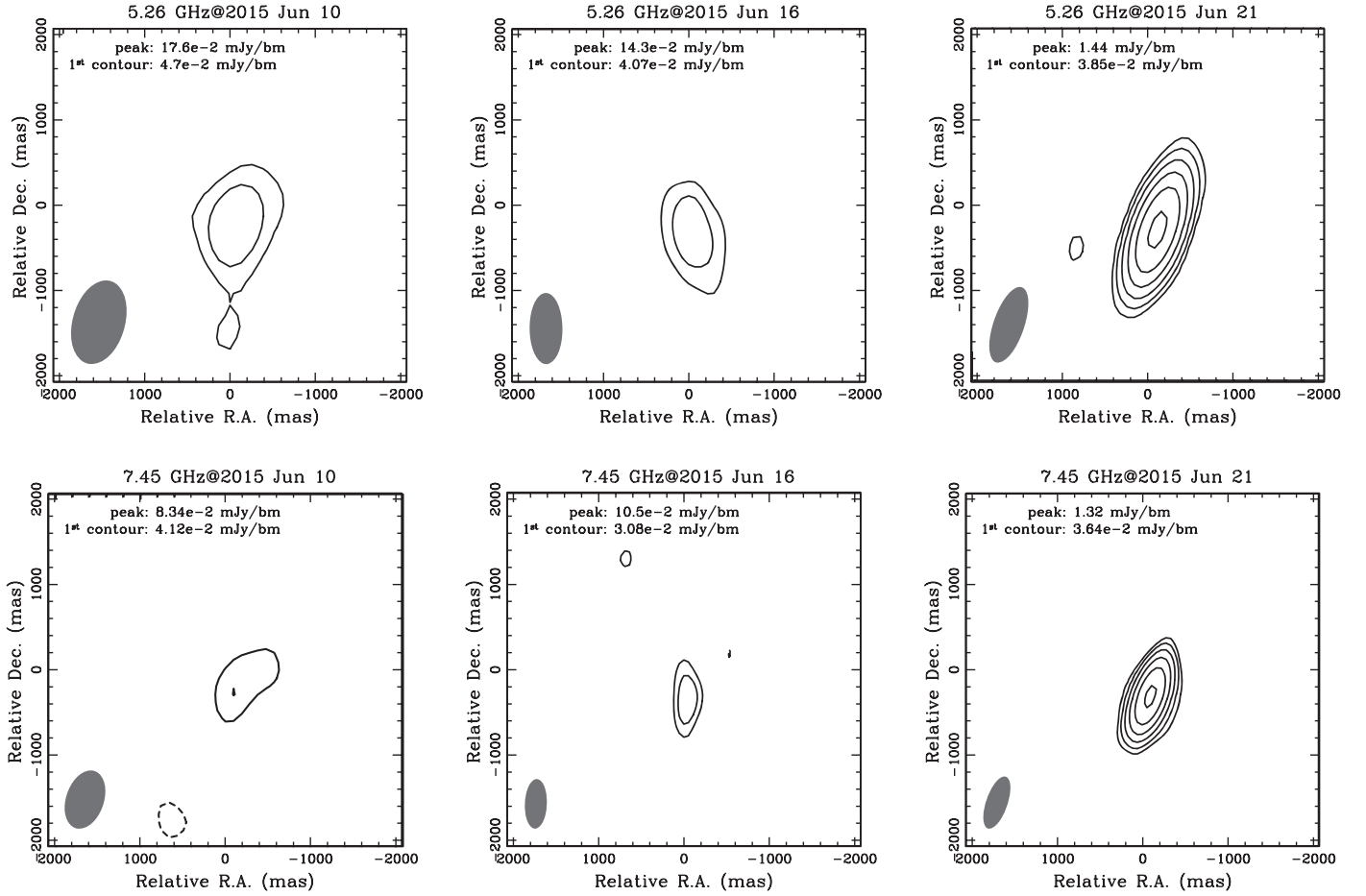
**Figure 2.** VLA radio image of GRS 1739–278 at 5.26 GHz (top panels) and 7.45 GHz (bottom panels). The plots center at R.A. = 17$^h$42$^m$40$^s$030 and decl. = −27° 44′52″699. From left to right, they are, respectively, on 2015 June 10 (MJD 57183, hard state), 2015 June 16 (MJD 57189, intermediate state), and 2015 June 21 (MJD 57194, soft state). The shadow in each panel shows the beam size (FWHM). The peak flux per beam ("bm" in the figure) as well as the the first (solid curve) contour are labeled in each panel. The contours increases by a factor of 2, i.e., they follow (−1, 1, 2, 4, 8, ...).

Besides, as shown in Figure 2, we find that the radio location of GRS 1739–278, determined by the VLA observations in A configuration, whose spatial resolution is higher than that in C configuration, systematically shifts by 78.5 mas in R.A. and −313.9 mas in decl., i.e., the actual position of GRS 1739–278 determined by VLA on 2015 June 21 (brightest in radio) is

$$\text{R. A. (J2000)} = 17^h42^m40^s022 \pm 0^s002,$$
$$\text{decl. (J2000)} = -27°44′52″981 \pm 0″005. \qquad (1)$$

Here we only include the statistical errors on the fit of beam centroiding, i.e., evaluated as $\text{beam}/2 \times S_{\text{peak}}/\sigma_{\text{rms}}$.

The middle and bottom panels of Figure 1 show, respectively, the lightcurve and the spectral index in radio. Consistent with other BHBs in hard state, the radio spectrum of the hard state in GRS 1739–278 is typically thick. There are several hard-state epochs whose radio spectrum seems steep (optically thin), i.e., on 2015 June 10 (MJD 57183, see also the left panels in Figure 2 for radio images) and on 2016 September 30 (MJD 57661). If real, they may possibly relate to the episodic ejections in the hard state (Yuan et al. 2009a) or the quiescent state (e.g., in our Galaxy center Sgr A*, Dodds-Eden et al. 2011). However, as shown in Figure 1, the value of $\alpha$ at these epochs is not firmly measured, we thus avoid further discussions.

### 3.2. Radio Evolution in Intermediate and Soft States

We here focus on the radio evolution in intermediate and soft states. The radio evolution in the hard state will be addressed subsequently in Section 3.3.

Due to the sparse schedule of the radio monitoring, we unfortunately did not catch the jet evolution in the intermediate state during the rise phase of the first mini-outburst (around MJD 57180–57190). Instead, we have two epochs of intermediate state observations during the rise phase of the second mini-outburst (around MJD 57240–57250; see Figure 1), where we likely observe an unfinished jet quenching process within 5 days, i.e., with an increase in X-ray flux by a factor of ∼3, the radio flux reduces by a factor of ∼12 at 5.26 GHz and ∼18 at 7.45 GHz, from MJD 57242 to MJD 57247 (i.e., during the hard-to-soft state transition). Meanwhile, the radio spectrum also steepens, consistent with transient ejections. We note the jet quenching during the state transition is commonly observed in main outbursts (e.g., Fender et al. 1999; Coriat et al. 2011), and it has also been observed during the state transition of mini-outbursts in another BH transient MAXI J1535–571 (Parikh et al. 2019).

Among all the 32 epochs of radio observations, there is only one epoch, i.e., on 2015 June 21 (MJD 57194), that the system
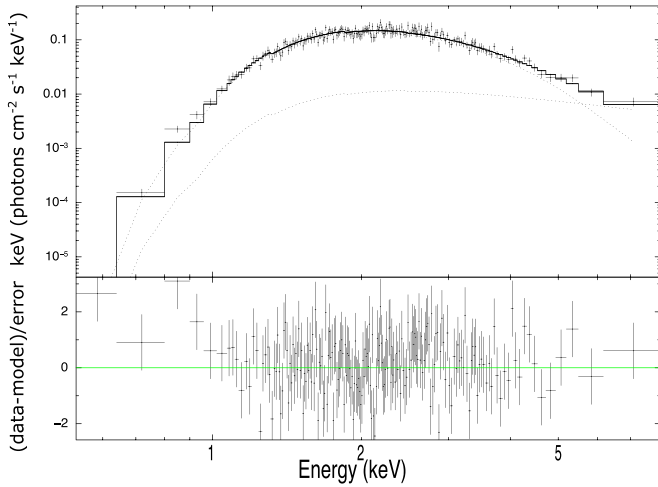
**Figure 3.** The spectral modeling of the X-ray spectrum of GRS 1739–278 on MJD 57194. In the upper panel, the two dotted curves are the absorbed emission of *diskbb* (upper one at 5 keV) and *powerlaw* (lower one at 5 keV), and the solid curve represents the sum.

is in the soft state.[6] The X-ray observations show that this source entered into the soft state about 3 days ago, on MJD 57191 (more accurately, between MJD 57190.48 and MJD 57191.67, see Figure 1 and Yan & Yu 2017b.). As shown in Figure 3, the X-ray spectrum on MJD 57194 is well-fitted under the adopted model, where the disk component contributes ≈88% of total flux in 1–10 keV. The best-fit values of the inner disk temperature and the photon index are $T_{in} = 0.66^{+0.03}_{-0.01}$ keV and $\Gamma = 2.13^{+0.93}_{-0.44}$, respectively. All these properties justify our soft state classification on MJD 57194. In this soft state (on MJD 57194) the system reaches maximal radio flux among all the 32 radio observations. Besides, the radio emission is spatially unresolved (see the right panels of Figure 2) and the radio spectrum is marginally optically thick, with $\alpha \approx -0.28 \pm 0.17$ (see Figure 1).

### 3.3. Radio/X-Ray Correlation in Hard State

We now investigate the relationship between luminosities in 5 GHz radio and 1–10 keV X-rays for GRS 1739–278. As shown in Figure 4, observations in hard state are focused. In this plot, the 2015–2016 mini-outbursts are shown by blue squares, where optically thick (spectral index clusters around $\alpha \approx -0.2$) and optically thin ($\alpha$ clusters around $\alpha \sim -1$) data points are shown, respectively, in filled and open symbols. We also show in this plot data points in soft (red squares) and intermediate (green squares) states of GRS 1739–278. For comparison, we also show the RX correlation of other BHBs in their hard states, where the data are taken from the latest compilation of Bahramian et al. (2018).[7] Sources that follow the standard $p \approx 0.61$ correlation (Corbel et al. 2013, the black dashed curve for the fit) are shown by black filled circles, and those that follow the hybrid correlation (Coriat et al. 2011, the blue dotted–dashed curve for the fit of the $p \approx 1.3$ branch) are shown by the black filled triangles.

Several results can be derived immediately. First, we find that for GRS 1739–278, there is no clear difference between
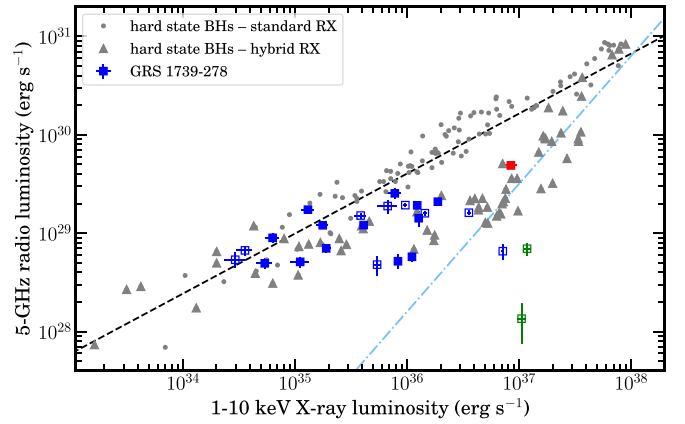


**Figure 4.** Radio/X-ray correlation. The squares show the data of GRS 1739–278, with color following Figure 1. Here the filled ones are optically thick and the open ones are optically thin. Data of other BHBs, compiled by Bahramian et al. (2018), are shown by gray filled circles and triangles, respectively, for standard ($p \approx 0.61$, see Corbel et al. 2013 and the black dashed curve for the fitting) and hybrid (see Coriat et al. 2011, and blue dotted–dashed for the $p \approx 1.3$ branch) RX correlations. The colors of data points of GRS 1739–278 are the same to those of Figure 1.

optical-thick jets and optical-thin ones. Second, the radio flux varies with a rather large scatter at a given X-ray luminosity, with a weak hint on the existence of two tracks, one is systematically fainter than the other by a factor of ~4 at given X-ray luminosity. However, the evidence of two tracks is weak. Below we omit this separation.

Third, apart of the large scatters, the RX relationship in GRS 1739–278 shows a clear deviation to the standard $p \approx 0.61$ one. We run a linear fit between $\log L_R$ and $\log L_X$ for all the data points in the hard state (including both optical-thick ones and optical-thin ones) and the result is

$$\log(L_R /\mathrm{erg\ s^{-1}}) = (0.16 \pm 0.09)\log(L_X /\mathrm{erg\ s^{-1}}) \\ + 23.3 \pm 3.1, \qquad (2)$$

i.e., for a range of more than two orders of magnitude in X-ray luminosity this source exhibits a rather flat RX correlation. Interestingly, H1743–322 also follows a flat correlation in this X-ray luminosity regime (transition regime in the notation of Coriat et al. 2011), and the dynamical range in X-ray luminosity of this flat correlation branch is also similar to our results, see Coriat et al. (2011).

For a detailed RX correlation investigation of GX 339-4, Fürst et al. (2015) find that the rise and decay phases of outbursts follow different tracks (see also Islam & Zdziarski 2018). To examine this possibility in GRS 1739–278, we in Figure 5 separate the rise and decay phases by the solid and open squares, respectively. Note that because of the hysteresis phenomenon, the X-ray luminosity of the rise phase is systematically brighter than that of the decay phase. Except of this difference, there is no clear difference in the RX correlation among these two phases, especially when the large scatters in the data points are considered.

### 4. Summary and Discussions

#### 4.1. Summary

In this work, we analyzed the VLA radio observations of the 2015–2016 mini-outbursts of GRS 1739–278. The VLA monitoring campaign has simultaneous detections at 5 and

---

[6] The epoch on 2015 June 26 (MJD 57199) is a soft state candidate, where a steep radio spectrum ($\alpha = -2.13 \pm 1.0$) is observed. But without X-ray observation the spectral state cannot be confirmed (see Table 1).
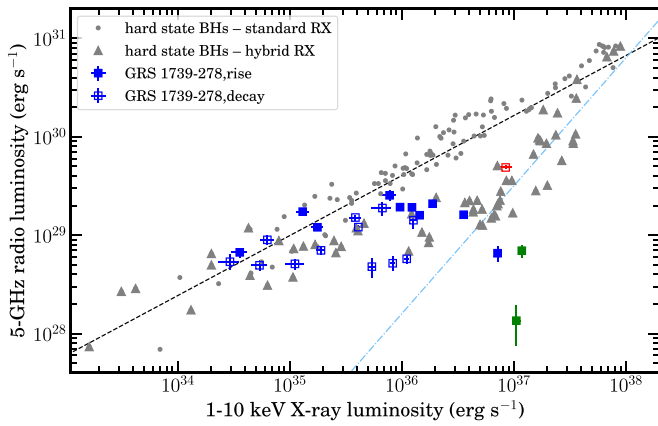[7] https://github.com/bersavosh/XRB-LrLx_pub

**Figure 5.** Radio/X-ray correlation. This plot is the same as that in Figure 4, except that the rise and decay phases of GRS 1739–278 are shown separately by filled (rise phase) and open (decay phase) squares.

8 GHz, and runs from 2015 June 10 until 2016 October 31. Among the 32 epochs, 25 epochs have quasi-simultaneous X-ray observations by *Swift*/XRT within one day (see Table 1). The position of GRS 1739–278 constrained by our VLA observation in A configuration is R.A. = $17^h42^m40^s.022$ and decl. = $-27°44'52''.981$ in the J2000 coordinate.

The main results of this work can be summarized as follows:

1. The radio image of GRS 1739–278 remains unresolved in all our A-configuration VLA observations, whichever state it is and whatever spectral properties it has in radio band. No superluminal motion is observed in this source.

2. A majority of radio observations in the hard state show an optically thick spectrum, consistent with previous findings (see Fender et al. 2004, 2009; Fender & Gallo 2014 for reviews). Occasionally the radio spectrum in the hard state becomes optically thin, and the spectrum can be as steep as $\alpha \sim -1$, but admittedly the uncertainties in $\alpha$ are large.

3. The jet quenching process is possibly caught during the intermediate state of the rise phase of the outburst, which represents an ongoing stage of hard-to-soft transition. On the other hand, we also spot an optically thick ($\alpha \approx -0.28 \pm 0.17$) radio emission in the soft state, which turns out to be the brightest among all the VLA epochs.

4. For the RX correlation during the hard state, there is no clear difference between optical-thin jets and optical-thick ones. Moreover, for more than two orders of magnitude in the variation of X-ray luminosity, GRS 1739–278 follows a flat RX correlation with $p \approx 0.16 \pm 0.09$. Both the correlation slope and the X-ray luminosity regime agree well with the hybrid RX prototype H1743–322 (Coriat et al. 2011), although neither the $p \approx 1.3$ correlation branch at the bright $L_X$ part nor the recover to the standard correlation branch at the faint $L_X$ part are observed in this source. Coordinated monitoring campaign in radio and X-rays of main and mini-outbursts in the future is in demand to examine the connection (and possibly the difference) among these two sources.

### 4.2. Radio Emission in the Soft State

Only on 2015 June 21 is the system confirmed to be in the soft state, during which a very bright but marginally optically thick ($\alpha \approx -0.28 \pm 0.17$) radio emission is detected. It remains unresolved in VLA (A-configuration).

The radio emission in soft state, if observable, usually exhibits a steep optically thin spectrum (see, e.g., Fender et al. 2004, 1999; Yuan et al. 2009a; Russell et al. 2019), which is produced by the residual episodic jet that launched during the hard-to-soft state transitions (see Section 1). It can be fairly bright if the ejecta interacts with dense medium (e.g., with stellar wind in Cyg X-3, see, e.g., Koljonen et al. 2010). In GRS 1739–278 such optical-thin radio emission in the soft state is indeed observed on MJD 57199 (see Section 3.1) and during the 1996 main outburst (Hjellming 1997). The soft state of the 1996 outburst, crudely identified from the hardness ratio measurement in X-rays by *RXTE*/ASM, lasts over 170 days (between MJD 50166 and MJD 50338). VLA observations reveal that the radio emission is always optically thin during this period (Hjellming 1997).

We note that, in the episodic ejection model a flat spectrum can be observed at the early phase, when the ejecta is small and dense, thus synchrotron self-absorption peaks at a higher frequency. However, this implies that the radio emission peaks on some later day. Considering the low radio flux 5 days later on MJD 57199 (i.e., the candidate soft state), an efficient cooling of the relativistic electrons and/or decline in magnetic field strength in the ejecta will be necessary. For the soft state radio observation on MJD 57194 (2015 June 21), we thus disfavor the episodic ejection during the state transition, but instead favor the interpretation of an optically thick emission from a continuous jet.

Among all the BHBs discovered so far, to our knowledge the only other source with a continuous jet in the soft state is Cyg X-3 (Zdziarski et al. 2018), where a radio-to-X-ray time lag of ~50 days is also observed. However, Cyg X-3 is a well-known high-mass X-ray binary, and the accumulation of magnetic flux supplied by the high-mass companion in the soft state is argued to be crucial for the launch of a jet in the soft state (Cao & Zdziarski 2020). This mechanism cannot operate in low-mass binaries like GRS 1739–278 (Cao & Zdziarski 2020).

Our detection of the optically thick radio emission during the soft state may imply that we possibly find in BHBs the counterpart of radio-loud AGNs (and quasars) that also have continuous jets. These systems are high in Eddington ratio $L_{bol}/L_{Edd}$ (Eddington luminosity for a BH with mass $M_{BH}$ is, $L_{Edd} = 1.3 \times 10^{46}(M_{BH}/10^8\,M_\odot)$ erg s$^{-1}$), and are dominated by thermal emission from a cold disk, as the case of the soft state in BHBs. Intense coordinated monitoring in radio and X-rays during the soft state in the future are necessary to verify it.

### 4.3. Theoretical Interpretation of Radio/X-Ray Correlation

The physical reason for the hybrid RX correlation, as well as its connection to the standard one, remain poorly understood. Several scenarios have been proposed in the literature. Below we examine our data with these existing models.

The first scenario of the hybrid RX emphases on the difference between the rise and the decay phases of the outburst. Islam & Zdziarski (2018) analyzed the evolution of H1743–322 and GX 339-4, where they reported that the

different branches in the hybrid RX correlation relate to the evolutionary phases (rise or decay) of the outburst, i.e., the $p \approx 1.3$ branch is achieved during the rise phase, while the $p \sim 0$ branch is established during the decay phase. However, this model is disfavored by observations in GRS 1739–278. In this source, both the rise and the decay phases are observed. But as shown in Figure 5, no clear difference in the slope of the RX correlation among the two phases is observed.

Espinasse & Fender (2018) took another approach. They separated the radio-loud sources from the radio-quiet ones based on their RX correlations, and investigated the distribution of radio spectral indices within each subsample. Note that the radio-loud and -quiet ones correspond to, respectively, the standard and the hybrid RX ones in our classification. Espinasse & Fender (2018) found that the spectral index of the radio-quiet subsample (hybrid RX sources), $\alpha \approx -0.2$, is systematically lower than that of the radio-loud subsample (standard RX sources), $\alpha \approx 0.2$ (see also Brocksopp et al. 2013 for a hint of such difference). This interpretation agrees with our data. According to their classification, GRS 1739–278 is a radio-quiet system, where a clustering of $\alpha$ at $\alpha \sim -0.2$ is observed in the hard state. We caution that epochs of even steeper radio spectrum (i.e., $\alpha \sim -1$) are observed in GRS 1739–278 in its hard state, although the spectral index of these observations suffers large uncertainties, see Figure 1.

The above two scenarios are motivated by observations. There is another one that is motivated by the progress on the fundamental properties of accretion physics, i.e., the radiative efficiency of hot accretion flow (Xie & Yuan 2016; see Cao et al. 2014; Meyer-Hofmeister & Meyer 2014; Qiao & Liu 2015 for the $p \approx 1.3$ branch only, and Coriat et al. 2011 for the efficiency requirement from observations). One advantage of this interpretation is that it is based on the truncated accretion–jet model (Esin et al. 1997; Yuan & Narayan 2014), which has been successfully applied to the hard state of BHBs. In this model, the synchrotron radio emission from a jet follows $L_R \propto \dot{M}_{jet}^{\sim 1.4}$ (Heinz & Sunyaev 2003), where $\dot{M}_{jet}$ the mass-loss rate into the jet. If the X-ray emission from hot accretion flow scales with mass accretion rate $\dot{M}$ as $L_X \propto \dot{M}^k$ (parameter $k$ characters the radiative efficiency in X-rays) and $\dot{M}_{jet} \propto \dot{M}$, then we have $L_R \propto L_X^{\sim 1.4/k}$ (Heinz & Sunyaev 2003; Coriat et al. 2011). In this picture, different slope in RX correlation is due to the difference in $k$, i.e., the standard one has $k \approx 2.2$ (Esin et al. 1997; Merloni et al. 2003), flat $p \sim 0$ one has $k \gg 1$, and $p \approx 1.3$ has $k \approx 1$. Interestingly, such a change in $k$ is indeed observed in hot accretion flows, where depending on $\dot{M}$ three distinctive accretion modes are found (Xie & Yuan 2012). We emphasize that the change in accretion mode will also result in a change in the spectral properties, which is confirmed in both BHBs and AGNs (see, e.g., Yang et al. 2015; Li 2019; Ruan et al. 2019).

This efficiency-related model by Xie & Yuan (2016) also predicts that the viscosity parameter of hot accretion flow, $\alpha_{hot}$, should be small in hybrid RX sources (e.g., BHB H1743–322: Xie & Yuan 2016, and AGN NGC 7213: Xie et al. 2016). Although $\alpha_{hot}$ is difficult to measure, it can be crudely estimated from the critical luminosity of the hard-to-soft state transition $L_{crit}$, since theoretically we have $\alpha_{hot} \propto L_{crit}^{\sim 1}$ (Xie & Yuan 2012; Xie et al. 2016). Interestingly, both GRS 1739–278 and MAXI J1535–571 (Parikh et al. 2019; Russell et al. 2019) are hybrid RX sources with state transitions observed in the mini-outbursts, thus they agree well with this predication.

### 4.4. Disk–Jet Coupling During the Mini-outbursts

So far the disk–jet coupling during the mini-outbursts has been investigated only in two BH transients: one is GRS 1739–278 in this work, the other is MAXI J1535–571 in Parikh et al. (2019). In both systems, the peak luminosities and durations of these mini-outbursts are at least one order of magnitude smaller than those of the main outburst, but still have state transitions at such low luminosities (Yan & Yu 2017b; Parikh et al. 2019). Besides, the hard-to-soft state transition luminosity and the peak luminosity follows the same correlation that is established in the main outbursts of BHBs, implying that there is no intrinsic physical difference among these two types of outbursts (Yan & Yu 2017b).

The jet properties in those short-duration mini-outbursts are also similar to those in main outbursts. There is no radio observation of GRS 1739–278 during the hard state of the main outburst, but observations of MAXI J1535–571 (Parikh et al. 2019) suggest that both the main and the mini-outbursts follow the hybrid RX correlation in the hard state. Moreover, considering the difference in the X-ray luminosity among main and mini-outbursts, the $p \approx 1.3$ branch of the hybrid RX correlation may only exist in the main outburst, see the case of MAXI J1535–571 (Russell et al. 2019, admittedly there are only two data points).

### ORCID iDs

Fu-Guo Xie ⍟ https://orcid.org/0000-0001-9969-2091
Zhen Yan ⍟ https://orcid.org/0000-0002-5385-9586
Zhongzu Wu ⍟ https://orcid.org/0000-0001-8577-132X

### References

Bahramian, A., Miller-Jones, J., Strader, J., et al. 2018, Radio/X-ray correlation database for X-ray binaries v0.1, Zenodo, doi:10.5281/zenodo.1252036
Bell, M. E., Tzioumis, T., Uttley, P., et al. 2011, MNRAS, 411, 402
Belloni, T. M. 2010, in The Jet Paradigm, ed. T. Belloni (Berlin: Springer-Verlag), 53
Borozdin, K., & Trudolyubov, S. P. 2000, ApJL, 533, L131
Brocksopp, C., Corbel, S., Tzioumis, A., et al. 2013, MNRAS, 432, 931
Cao, X., & Zdziarski, A. A. 2020, MNRAS, 492, 223
Cao, X. F., Wu, Q., & Dong, A. J. 2014, ApJ, 788, 52
Corbel, S., Coriat, M., Brocksopp, C., et al. 2013, MNRAS, 428, 2500
Corbel, S., Fender, R. P., Tomsick, J. A., et al. 2004, ApJ, 617, 1272
Corbel, S., Fender, R. P., Tzioumis, A. K., et al. 2000, A&A, 359, 251
Corbel, S., Fender, R. P., Tzioumis, A. K., et al. 2002, Sci, 298, 196
Corbel, S., Nowak, M. A., Fender, R. P., Tzioumis, A. K., & Markoff, S. 2003, A&A, 400, 1007
Coriat, M., Corbel, S., Prat, L., et al. 2011, MNRAS, 414, 677
Dincer, T., Bailyn, C. D., Miller-Jones, J. C. A., Buxton, M., & MacDonald, R. K. D. 2018, ApJ, 852, 4
Dodds-Eden, K., Gillessen, S., Fritz, T. K., et al. 2011, ApJ, 728, 37

Done, C., Gierlinski, M., & Kubota, A. 2007, A&Ar, 15, 1
Dong, A. J., Wu, Q., & Cao, X. F. 2014, ApJL, 787, L20
Durouchoux, P., Smith, I. A., Hurley, K., et al. 1996, IAUC, 6383, 1
Esin, A. A., McClintock, J. E., & Narayan, R. 1997, ApJ, 489, 865
Espinasse, M., & Fender, R. 2018, MNRAS, 473, 4122
Falcke, H., Körding, E., & Markoff, S. 2004, A&A, 414, 895
Fender, R. P., Belloni, T. M., & Gallo, E. 2004, MNRAS, 355, 1105
Fender, R. P., & Gallo, E. 2014, SSRv, 183, 323
Fender, R. P., Garrington, S. T., McKay, D. J., et al. 1999, MNRAS, 304, 865
Fender, R. P., Homan, J., & Belloni, T. M. 2009, MNRAS, 396, 1370
Fürst, F., Nowak, M. A., Tomsick, J. A., et al. 2015, ApJ, 808, 122
Fürst, F., Tomsick, J. A., Yamaoka, K., et al. 2016, ApJ, 832, 115
Gallo, E., Fender, R. P., & Pooley, G. G. 2003, MNRAS, 344, 60
Gallo, E., Miller, B. P., & Fender, R. P. 2012, MNRAS, 423, 590
Gallo, E., Miller-Jones, J. C. A., Russell, D. M., et al. 2014, MNRAS, 445, 290
Greiner, J., Dennerl, K., & Predehl, P. 1996, A&A, 314, L21
Gültekin, K., Cackett, E. M., Miller, J. M., et al. 2009, ApJ, 706, 404
Gültekin, K., King, A. L., Cackett, E. M., et al. 2019, ApJ, 871, 80
Heinz, S. 2004, MNRAS, 355, 835
Heinz, S., & Sunyaev, R. A. 2003, MNRAS, 343, L59
Hjellming, R. M. 1997, in IAU Coll. 163, Accretion Phenomena and Related
     Outflows, ed. D. T. Wickramasinghe, G. V. Bicknell, & L. Ferrario
     (Cambridge: Cambridge Univ. Press), 53
Hjellming, R. M., & Rupen, M. P. 1995, Natur, 375, 464
Islam, N., & Zdziarski, A. A. 2018, MNRAS, 481, 4513
Jonker, P. G., Miller-Jones, J. C. A., Homan, J., et al. 2012, MNRAS,
     423, 3308
King, A. L., Miller, J. M., Reynolds, M. T., et al. 2013, ApJL, 774, L25
King, A. L., Miller, J. M., Cackett, E. M., et al. 2011, ApJ, 729, 19
Koljonen, K. I. I., Hannikainen, D. C., McCollough, M. L., Pooley, G. G., &
     Trushkin, S. A. 2010, MNRAS, 406, 307
Krimm, H. A., Barthelmy, S. D., Baumgartner, W., et al. 2014, ATel, 5986, 1
Li, S. L. 2019, MNRAS, 490, 3793
Li, S. L., & Gu, M. 2018, MNRAS, 481, L45
Li, Z. Y., Wu, X. B., & Wang, R. 2008, ApJ, 688, 826
McMullin, J. P., Waters, B., Schiebel, D., Young, W., & Golap, K. 2007, in
     ASP Conf. Ser. 376, Astronomical Data Analysis Software and Systems
     XVI, ed. R. A. Shaw, F. Hill, & D. J. Bell (San Francisco CA: ASP), 127
Merloni, A., Heinz, S., & di Matteo, T. 2003, MNRAS, 345, 1057
Meyer-Hofmeister, E., & Meyer, F. 2014, A&A, 562, 142

Mezcua, M., Hlavacek-Larrondo, J., Lucey, J. R., et al. 2018, MNRAS,
     474, 1342
Miller, J. M., Tomsick, J. A., Bachetti, M., et al. 2015, ApJL, 799, L6
Mirabel, I. F., & Rodriguez, L. F. 1994, Natur, 371, 46
Nyland, K., Davis, T. A., Nguyen, D. D., et al. 2017, ApJ, 845, 50
Panessa, F., Barcons, X., Bassani, L., et al. 2007, A&A, 467, 519
Parikh, A. S., Russell, T. D., Wijnands, R., et al. 2019, ApJL, 878, L28
Parikh, A. S., Wijnands, R., Degenaar, N., et al. 2018, ATel, 11869, 1
Plotkin, R. M., Miller-Jones, J. C. A., Gallo, E., et al. 2017, ApJ, 834, 104
Qian, L., Dong, X. B., Xie, F. G., Liu, W., & Li, D. 2018, ApJ, 860, 134
Qiao, E., & Liu, B. F. 2015, MNRAS, 448, 1099
Remillard, R. A., & McClintock, J. E. 2006, ARA&A, 44, 49
Rodriguez, J., Urquhart, R., Plotkin, R. M., et al. 2020, ApJ, 889, 58
Ruan, J. J., Anderson, S. F., Eracleous, M., et al. 2019, ApJ, 883, 76
Russell, D. M., Miller-Jones, J. C. A., Maccarone, T. J., et al. 2011, ApJL,
     739, L19
Russell, T. D., Tetarenko, A. J., Miller-Jones, J. C. A., et al. 2019, ApJ,
     883, 198
Shakura, N. I., & Sunyaev, R. A. 1973, A&A, 24, 337
Shepherd, M. C., Pearson, T. J., & Taylor, G. B. 1994, BAAS, 26, 987
Vargas, M., Goldwurm, A., Laurent, P., et al. 1997, ApJL, 476, L23
Wang, R., Wu, X. B., & Kong, M. Z. 2006, ApJ, 645, 890
Wang, S., Kawai, N., Shidatsu, M., et al. 2018, PASJ, 70, 67
Xie, F. G., & Yuan, F. 2012, MNRAS, 427, 1580
Xie, F. G., & Yuan, F. 2016, MNRAS, 456, 4377
Xie, F. G., & Yuan, F. 2017, ApJ, 836, 104
Xie, F. G., Zdziarski, A. A., Ma, R., & Yang, Q. X. 2016, MNRAS, 463, 2287
Yan, Z., & Yu, W. 2017a, ATel, 10137, 1
Yan, Z., & Yu, W. 2017b, MNRAS, 470, 4298
Yang, J., Brocksopp, C., Corbel, S., et al. 2010, MNRAS, 409, L64
Yang, Q. X., Xie, F. G., Yuan, F., et al. 2015, MNRAS, 447, 1692
Yao, S., Qiao, E., Wu, X.-B., et al. 2018, MNRAS, 477, 1356
Yuan, F., & Cui, W. 2005, ApJ, 629, 408
Yuan, F., Lin, J., Wu, K., et al. 2009a, MNRAS, 395, 2183
Yuan, F., & Narayan, R. 2014, ARA&A, 52, 529
Yuan, F., Yu, Z., & Ho, L. C. 2009b, ApJ, 703, 1034
Zdziarski, A. A., & Gierliński, M. 2004, PThPS, 155, 99
Zdziarski, A. A., Malyshev, D., Dubus, G., et al. 2018, MNRAS, 479, 4399
Zdziarski, A. A., Poutanen, J., Mikolajewska, J., et al. 1998, MNRAS,
     301, 435
Zhang, H., & Yu, W. 2015, MNRAS, 451, 1740